

# Electrostatic couplings in OmpA ion-channel gating suggest a mechanism for pore opening

Heedeok Hong, Gabor Szabo & Lukas K Tamm

The molecular forces that drive structural transitions between the open and closed states of channels and transporters are not well understood. The gate of the OmpA channel is formed by the central Glu52-Arg138 salt bridge, which can open to form alternate ion pairs with Lys82 and Glu128. To gain deeper insight into the channel-opening mechanism, we measured interaction energies between the relevant side chains by double-mutant cycle analysis and correlated these with the channel activities of corresponding point mutants. The closed central salt bridge has a strong interaction energy of  $-5.6 \text{ kcal mol}^{-1}$ , which can be broken by forming the open-state salt bridge Glu52-Lys82 ( $\Delta\Delta G_{\text{Inter}} = -3.5 \text{ kcal mol}^{-1}$ ) and a weak interaction between Arg138 and Glu128 ( $\Delta\Delta G_{\text{Inter}} = -0.6 \text{ kcal mol}^{-1}$ ). A covalent disulfide bond in place of the central salt bridge completely blocks the channel. Growth assays indicate that this gating mechanism could physiologically contribute to the osmoprotection of *Escherichia coli* cells from environmental stress.

Electrostatic interactions not only have important structural roles in proteins, but also participate in a variety of mechanisms that are important for protein function, for example protein-protein interactions, ligand binding, catalysis and allostery<sup>1-4</sup>. In general, electrostatic effects are more strongly manifested in membrane proteins than in water-soluble proteins because the lipid bilayer provides a low dielectric medium for membrane proteins<sup>5</sup>. Examples include electrostatically driven lateral associations of transmembrane receptor complexes<sup>6</sup>, activation of rhodopsin by remodeling of a specific salt bridge<sup>7</sup> and gating of ion channels by voltage<sup>8,9</sup>. However, the thermodynamics of the electrostatic interactions that induce reversible associations and activate molecular switches in membrane proteins have not yet been assessed. The absence of such measurements is mainly due to a lack of experimental methods for quantifying the strengths of such interactions. Here, we present the first thermodynamic study to measure electrostatic side chain interaction energies in an integral membrane protein and their implications for the protein's stability and function. We chose the outer membrane protein A (OmpA) from *E. coli* for these studies because it contains an electrostatically controlled core that can switch the central pore between an open and a closed state.

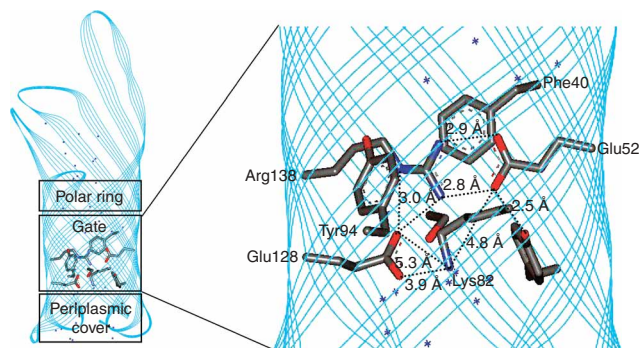
OmpA is an abundant protein of the outer membrane of Gram-negative bacteria, where it has an important structural role<sup>10,11</sup>. It consists of an N-terminal transmembrane domain (residues 1-171) and a C-terminal periplasmic domain (residues 172-325), which is linked to the peptidoglycan layer<sup>12</sup>. OmpA forms a small gated pore in membranes that is permeable to ions and larger solutes<sup>13-16</sup>. The protein also serves as a receptor for various phages and colicins and is a mediator of F factor-dependent conjugation<sup>17</sup>. Finally, OmpA from pathogenic bacteria plays a role at an early stage of their crossing of the blood-brain barrier and is thereby involved in the pathogenesis of meningitis<sup>18</sup>.

The three-dimensional structure of the OmpA transmembrane domain has been solved by X-ray crystallography and NMR<sup>19,20</sup>. It features an eight-stranded  $\beta$ -barrel with a polar, strongly hydrogen-bonded core and apolar residues facing the surrounding lipid bilayer. Although the central pore of OmpA is accessible to water from the outside, a cluster of charged residues consisting of Glu52, Arg138, Glu128 and Lys82 surrounded by aromatic side chains Tyr8, Phe40 and Tyr94 forms the main constriction or 'gate' in the middle of the protein (Fig. 1). A salt bridge between Glu52 and Arg138 crosses the barrel lumen through the center. There are two additional secondary constrictions above and below the central gate: a polar ring partially occludes the lumen on the extracellular side and an N-terminal cover blocks access from the periplasmic side (Fig. 1). Despite these constrictions, OmpA is permeable to ions and small organic solutes, as observed in numerous biochemical and electrophysiological studies<sup>13-16</sup>. However, the mechanism of pore opening and the biological significance of the pore's function are still poorly understood. To explain the pore activity of OmpA, some authors have proposed that Glu128, which is located below Arg138 on the same side of the barrel, may serve as an alternative salt-bridge partner for Arg138, thereby breaking the Glu52-Arg138 salt bridge and opening the gate to form a transiently open channel in the pore lumen of the barrel<sup>21</sup>. To support their model, these authors performed a molecular dynamics simulation with OmpA in the proposed open state. The modeled open-state salt bridge Glu128-Arg138 was stable during the applied simulation time of  $\sim 2 \text{ ns}$  and showed a calculated conductance similar to the experimentally measured value<sup>16</sup>.

In this study, we determined five thermodynamic pair-wise side chain interaction energies within the salt-bridge tetrad to identify which if any of these interactions are strong enough to open the

Department of Molecular Physiology and Biological Physics, University of Virginia Health System, PO Box 800736, Charlottesville, Virginia 22908-0736, USA. Correspondence should be addressed to L.K.T. (lkt2e@virginia.edu).

Received 12 June; accepted 30 August; published online 15 October 2006; doi:10.1038/nchembio827



Glu52-Arg138 gate. Because analysis by single mutations often cannot eliminate residual nonspecific interactions and the possibility of global structural changes of the protein, we used double-mutant cycle analysis combined with equilibrium unfolding for this purpose<sup>22</sup>. In parallel, we performed single ion-channel conductance measurements in planar lipid bilayers with wild-type and several mutants of OmpA in order to probe the contribution of each residue in the tetrad to the channel activity of OmpA. We also identified a double cysteine mutant, E52C R138C, that had the pore blocked under oxidizing but not reducing conditions, and we tested the physiological role of the OmpA channel using cell growth assays under osmotic stress. The results suggest that several electrostatic interactions contribute not only to the gating mechanism, but also to the stability of the OmpA pore, which apparently contributes to the protection of *E. coli* cells from osmotic stress.

## RESULTS

### Gate architecture and double-mutant cycle analysis

The hydrogen-bonded heavy atoms of the gating salt bridge Glu52-Arg138 in the center of OmpA are separated by 2.8 to 2.9 Å (Fig. 1)<sup>23</sup>. This salt bridge is sandwiched between Phe40 and Tyr94, which occupy a substantial volume in the gating region. Arg138 is further hydrogen bonded to Glu128 (distance 3.0 Å), but Lys82, which electrostatically neutralizes the charge tetrad in the gate, is too far from Glu52 (4.8 Å) and Glu128 (3.9 Å) to form hydrogen bonds with these residues. Instead Tyr8 is hydrogen bonded to Glu52 (2.5 Å). These gate residues are all strictly conserved throughout the OmpA family of outer-membrane proteins<sup>19</sup>. To distinguish among different possible gating mechanisms, we set up eight double-mutant cycles,

**Figure 1** Configuration of side chains in the gate region of OmpA, based on the high-resolution crystal structure of its transmembrane domain. The lumen of the barrel is filled with polar side chains in the polar ring, gate and periplasmic cover regions according to their proposed roles in ion conduction (left). A number of ordered water molecules (marked with asterisks) are observed in the polar ring and the periplasmic cover region, but water is excluded from the gate region. A close-up of the gate shows an intricate hydrogen-bonding and salt-bridge network (right). Red and blue designate oxygen and nitrogen atoms, respectively.

which allowed us to measure the interaction energies of the five attractive side chain interactions (Glu52-Arg138, Glu128-Arg138, Tyr8-Glu52, Glu52-Lys82 and Lys82-Glu128) that each could potentially contribute to the gating of the OmpA ion channel. The strategy of this approach, which was originally developed for the measurement of pair-wise side chain interaction energies in soluble proteins<sup>22</sup>, is to mutate each of the interacting residues, designated X and Y, of protein P into noninteracting side chains (for example, alanines) in single and double mutants, and to measure the free energies of unfolding,  $\Delta G_{u,H_2O}^0$ , of wild type (P-XY), both single mutants (P-X and P-Y) and the double mutant (P). The interaction energy,  $\Delta\Delta G_{Inter}$  between X and Y is then determined from a thermodynamic cycle that is constructed from the free energies of unfolding of all four species<sup>22</sup>:

$$\Delta\Delta G_{Inter} = -[\Delta G_{u,H_2O}^0(P-XY) - \Delta G_{u,H_2O}^0(P-X)] + [\Delta G_{u,H_2O}^0(P-Y) - \Delta G_{u,H_2O}^0(P)] \quad (1)$$

which under the assumption that the two residues of interest are not interacting in the unfolded state is equivalent to

$$\Delta\Delta G_{Inter} = -[\Delta G_{P-XY \rightarrow P-X} - \Delta G_{P-Y \rightarrow P}] \quad (2)$$

where  $\Delta G_{P-XY \rightarrow P-X}$  is the free-energy difference between the folded states of wild type and mutant P-X and  $\Delta G_{P-Y \rightarrow P}$  is the free-energy difference between the folded states of mutant P-Y and double-mutant P. Our mutation scheme for double-mutant cycle analysis of the gating region of OmpA was to change the glutamates to glutamine or alanine, the arginine and lysine to alanine, and tyrosine to phenylalanine. In this scheme, the Glu52-Arg138, Glu128-Arg138 and Glu52-Lys82 interactions are each analyzed with two different sets of mutant proteins, whereas all other interactions are probed with single sets of mutants.

### Reversible two-state folding of wild type and mutants

Tryptophan fluorescence (Fig. 2a) and far UV CD (Fig. 2b) spectra of the first set of mutants (E52Q, R138A and E52Q R138A) were not

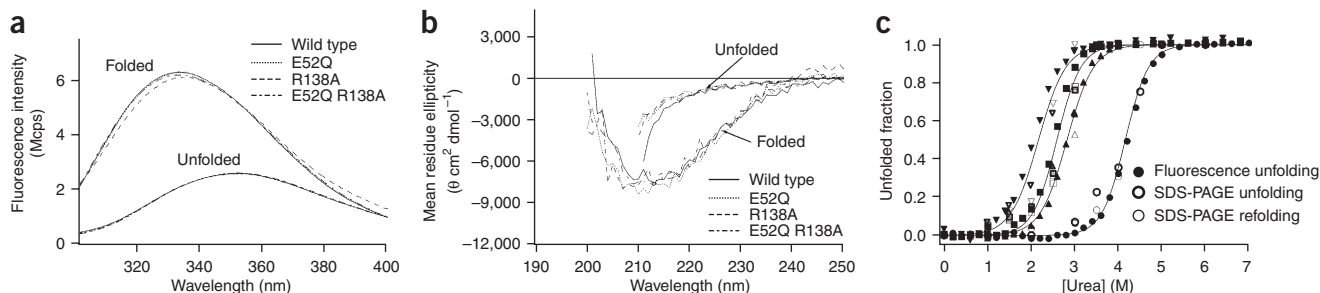


**Figure 2** Comparison of the structural and folding properties of wild-type and several mutant OmpAs in *d*/C<sub>16:1</sub>PC:C<sub>16:0</sub>C<sub>18:1</sub>PG (89.5:10.5) bilayers at 37.5 °C, pH 9.2. (a,b) Fluorescence (a) and far UV CD spectra (b) of the folded and unfolded states of wild-type and mutant proteins in lipid bilayers. Mcps, 10<sup>6</sup> counts per second. (c) Comparison of the folding and unfolding curves monitored by the SDS-PAGE shift assay to the unfolding curves monitored by the average emission wavelength for wild-type and mutant OmpAs. ●, wild type; ▲, E52Q R138A; ■, E52Q; ▼, R138A. Solid symbols, fluorescence unfolding; half-open symbols, SDS unfolding; open symbols, SDS refolding.

**Table 1** Thermodynamic parameters of solvent-induced unfolding

	$C_m$ (M)	$m$ (kcal mol <sup>-1</sup> M <sup>-1</sup> )	$\Delta G_{u,H_2O}^0$ (kcal mol <sup>-1</sup> )	$\Delta\Delta G_{u,H_2O}^0$ <sup>a</sup> (kcal mol <sup>-1</sup> )
Wild-type OmpA	4.2	2.2 ± 0.1	9.3 ± 0.2	0
E52A	1.9	2.3 ± 0.1	4.4 ± 0.2	4.9 ± 0.3
R138A	2.0	1.9 ± 0.1	3.8 ± 0.2	5.5 ± 0.3
E52A R138A	2.1	2.2 ± 0.1	4.5 ± 0.1	4.8 ± 0.2
E52Q	2.5	2.5 ± 0.1	6.4 ± 0.1	2.9 ± 0.2
E52Q R138A	2.8	2.3 ± 0.1	6.6 ± 0.2	2.7 ± 0.3
E128A	3.2	3.0 ± 0.1	9.4 ± 0.4	-0.1 ± 0.4
E128A R138A	1.9	2.3 ± 0.1	4.5 ± 0.2	4.8 ± 0.3
E128Q	3.5	2.9 ± 0.1	10.0 ± 0.3	-0.7 ± 0.4
E128Q R138A	2.2	2.4 ± 0.1	5.2 ± 0.2	4.1 ± 0.3
K82A	1.9	1.8 ± 0.1	3.4 ± 0.2	5.9 ± 0.3
E52A K82A	1.2	1.7 ± 0.1	2.0 ± 0.1	7.3 ± 0.2
E52Q K82A	1.9	2.1 ± 0.1	4.0 ± 0.1	5.3 ± 0.2
K82A E128Q	2.1	2.7 ± 0.1	5.8 ± 0.2	3.5 ± 0.3
Y8F	3.3	3.0 ± 0.1	10.0 ± 0.3	-0.7 ± 0.4
Y8F E52Q	2.5	3.1 ± 0.1	8.0 ± 0.3	1.3 ± 0.4

<sup>a</sup>Difference free energy of unfolding of wild type minus mutant.

substantially different from those of wild type, which indicates that the mutants were properly refolded in lipid bilayers. The mutant proteins also showed mean conductance values that are very similar to those of wild type (see below), which implies that the overall structure of the native OmpA is not significantly affected by the mutations. Similar data were obtained for all other sets of mutants. All mutants also maintained the thermodynamic reversibility and two-state equilibrium folding behavior that has been previously observed for the wild-type protein<sup>24</sup>. Native and denatured samples of OmpA appear as two different forms on SDS-PAGE gels<sup>25</sup>. Folding and unfolding curves monitored by this method superposed on each other and closely followed unfolding curves measured by tryptophan fluorescence (Fig. 2c). Given that (i) the SDS-PAGE and fluorescence methods report on very different kinetic phases of OmpA folding and (ii) these signals have been used to distinguish among different kinetic folding intermediates<sup>25</sup>, the fact that no intermediates were observed in the current equilibrium folding experiments justifies an analysis using the two-state model of the mutant cycle data to obtain the thermodynamic stabilities of the wild-type and mutant proteins<sup>24</sup>.

### Thermodynamic stability of wild type and mutants

Equilibrium unfolding curves of all eight sets of mutants obtained by tryptophan fluorescence are shown in **Supplementary Figure 1** online. The free energies of unfolding, the difference free energies between wild-type and mutant OmpAs, and the cooperativity parameters  $m$  derived from these data by using the two-state model are listed in **Table 1**. The values of  $\Delta G_{u,H_2O}^0$  and  $m$  for the wild type, 9.3 kcal mol<sup>-1</sup> and 2.2 kcal mol<sup>-1</sup> M<sup>-1</sup>, respectively, are larger than

those previously measured<sup>24</sup>. The reason for this difference is that in the present work we chose a different bilayer system consisting of 89.5% 1,2-dipalmitoleoyl phosphatidylcholine (*di*C<sub>16:1</sub>PC) and 10.5% 1-palmitoyl-2-oleoyl phosphatidylglycerol (C<sub>16:0</sub>C<sub>18:1</sub>PG), compared with 92.5% 1-palmitoyl-2-oleoyl phosphatidylcholine (C<sub>16:0</sub>C<sub>18:1</sub>PC) and 7.5% C<sub>16:0</sub>C<sub>18:1</sub>PG for the bilayer system used in the previous work. The stability of OmpA is a strong function of the elastic properties of lipid bilayers<sup>24</sup>. *Di*C<sub>16:1</sub>PC bilayers have a higher lateral pressure in the hydrocarbon region and provide better hydrophobic matching conditions than the C<sub>16:0</sub>C<sub>18:1</sub>PC bilayers that were previously used as references. OmpA is also more stable at neutral than at basic pH (ref. 24). The more stabilizing bilayer composition of the present work brings even the most destabilizing mutants into the experimentally accessible range, so that their thermodynamic stabilities are directly comparable to those of the wild type in the same lipid background.

There are several notable features of the effects of the gate mutations on the thermodynamic stability of OmpA. First, mutation of the two positively charged residues Lys82 and Arg138 was most destabilizing (K82A,  $\Delta G_{u,H_2O}^0 = 3.4$  kcal mol<sup>-1</sup>; R138A,  $\Delta G_{u,H_2O}^0 = 3.8$  kcal mol<sup>-1</sup>). The  $m$  values of these mutants were also 0.3 to 0.4 kcal mol<sup>-1</sup> M<sup>-1</sup> less than those of the wild type. These two side chains clearly contribute substantially to the stability of OmpA. Second, there were two, or perhaps three, slightly stabilizing mutations: Y8F ( $\Delta G_{u,H_2O}^0 = 10.0$  kcal mol<sup>-1</sup>), E128Q ( $\Delta G_{u,H_2O}^0 = 10.0$  kcal mol<sup>-1</sup>) and E128A ( $\Delta G_{u,H_2O}^0 = 9.4$  kcal mol<sup>-1</sup>). These mutants also have the highest  $m$  values among all mutants that were tested. Tyr8 and Glu128

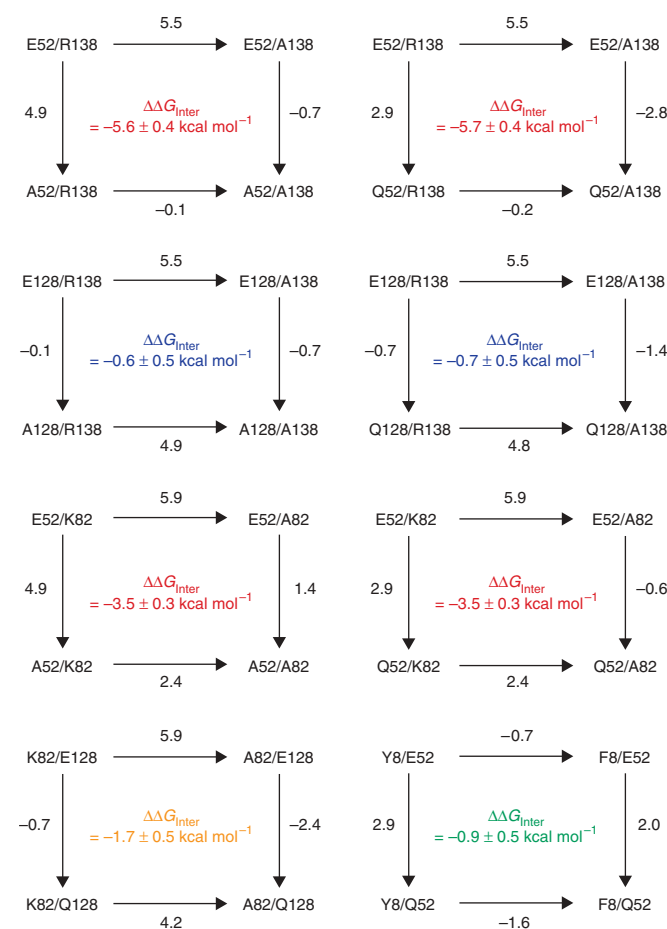


**Figure 3** Double-mutant cycles for estimating the interaction energies,  $\Delta\Delta G_{inter}$ , between the charged side chains in the gating region of the OmpA channel. The free-energy changes upon mutation (black numbers next to arrows) are calculated from the  $\Delta G_{u,H_2O}^0$  values of **Table 1** and the expressions in brackets of equation (1). The side chain interaction energies are calculated from the differences of parallel (horizontal or vertical) arrows in each cycle. Red, strong interactions; orange, intermediate interactions; green, intermediate-weak interactions; blue, weak interactions.

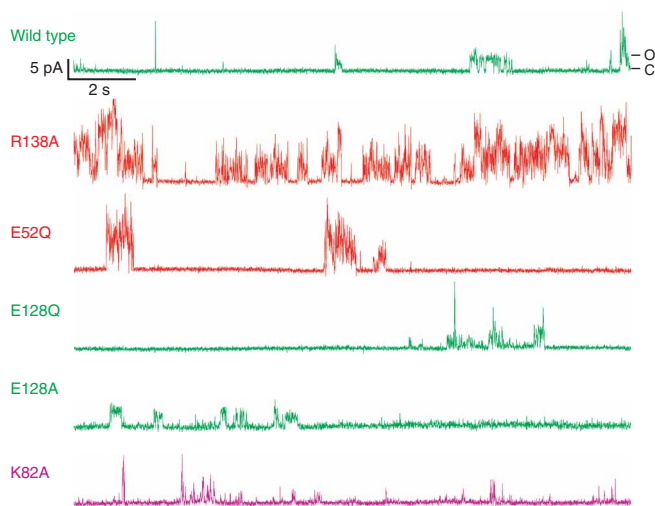


**Figure 4** Representative single-channel recordings of the small conductance states of wild-type and mutant OmpAs in planar lipid bilayers at +100 mV. Each 1.5-ml chamber was filled with 1 M KCl (10 mM Tris-HCl buffer, pH 7.4). 5  $\mu$ l of OmpA reconstituted in *d*C<sub>16:1</sub>PC (40  $\mu$ g ml<sup>-1</sup> at pH 9.2) was added to the grounded *cis* compartment, and a +100-mV potential was applied to the *trans* compartment after stirring. Green, same activity as wild type; red, more active than wild type; purple, less active than wild type.

are both directly adjacent to the Glu52-Arg138 salt bridge. Perhaps they abstract part of the local effective charge on either residue, or some hydrogen bonding power, from the Glu52-Arg138 ion pair and thereby weaken the strength of this salt bridge. Third, the alanine mutations that disrupt the Glu52-Arg138 salt bridge lead to a substantial destabilization of the protein. The free energies of unfolding of E52A and E52A R138A were 4.4 and 4.5 kcal mol<sup>-1</sup>, that is 4.9 and 4.8 kcal mol<sup>-1</sup> less than that of the wild type, respectively. However, E52Q and E52Q R138A were more moderately destabilized ( $\Delta G_{u,H_2O}^0 = 6.4$  and 6.6 kcal mol<sup>-1</sup>, respectively). Apparently, replacing Glu52 with glutamine did not completely abolish the hydrogen bonding interaction to Arg138, nor did it change other environmental interactions that may exist in the wild-type protein.

### Pair-wise interaction energy of gate residues

We calculated the interaction energies  $\Delta\Delta G_{\text{Inter}}$  between the eight pairs of side chains by constructing thermodynamic cycles (Fig. 3) and by using equation (1). The Glu52-Arg138 salt bridge had the strongest interaction energy,  $-5.6 \pm 0.4$  (s.d.) kcal mol<sup>-1</sup>. The interaction energies obtained from the two independent mutant cycle sets that probed this interaction agreed very well, which confirms that our methods are internally consistent. The interactions between the side chains that are closest to the central salt bridge and the residues of this salt bridge, that is Glu128-Arg138 and Tyr8-Glu52, were very weak ( $-0.6 \pm 0.5$  kcal mol<sup>-1</sup> and  $-0.9 \pm 0.5$  kcal mol<sup>-1</sup>, respectively). The interaction between the side chains of Glu52 and Lys82, which in the crystal structure are much farther apart from each other than the other pairs, turned out to be quite strong ( $\Delta\Delta G_{\text{Inter}} = -3.5 \pm 0.3$  kcal

mol<sup>-1</sup>). Finally, the interaction energy between Lys82 and Glu128 was  $-1.7 \pm 0.5$  kcal mol<sup>-1</sup>, which is intermediate between that of Glu52-Lys82 and Glu128-Arg138.

### Single-channel activity of wild type and mutants

To determine the roles of the relevant gate residues in the ion conduction mechanism, we performed single-ion-channel conductance measurements with wild-type and mutant OmpAs in 1,2-diphytanoyl phosphatidylcholine (*di*PhPC) planar bilayers. Figure 4 shows traces of representative recordings from the wild type and R138A, E52Q, E128Q, E128A and K82A mutant channels. The activity of wild type was characterized by current fluctuations with upward deflections of defined sizes. The conductance distribution from  $\sim 1,000$  analyzed opening events deviated from an ideal Gaussian distribution with a tail extending toward the higher conductance values, as is typical for these kinds of measurements (Fig. 5). The mean conductance value was  $28 \pm 22$  pS. The open-time distribution conformed to a Poisson distribution with a lifetime of the open state ( $\tau_{\text{open}}$ ) of  $102 \pm 4$  ms, a result obtained from a single-exponential fit

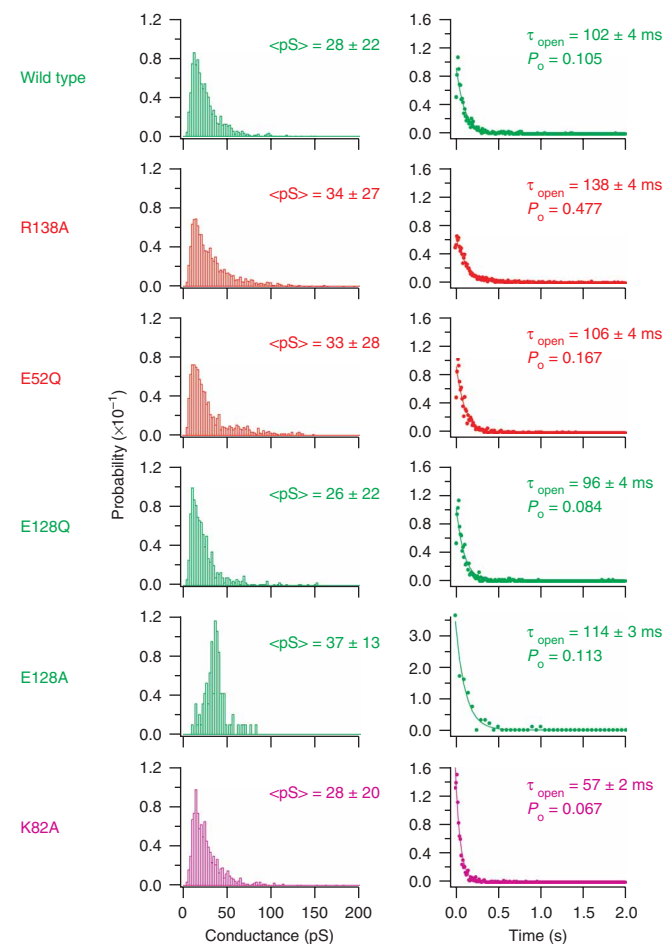


**Figure 5** Statistical analysis of the single-channel recordings of wild-type and mutant OmpAs in planar bilayers. The left column shows histograms of conductance distributions; the mean conductance values and s.d. are annotated in each graph. The right column shows lifetime distributions fitted to single exponential decays, which yielded the open-state lifetimes,  $\tau_{\text{open}}$ . The open probabilities,  $P_o$ , are defined as the fraction of time in which the channels are in the open state during the recorded time at +100 mV of applied voltage. Number of events analyzed: wild type, 984; R138A, 1,896; E52Q, 1,237; E128Q, 572; E128A, 94; K82A, 964. The channel characteristics of the mutants shown in green were not significantly different from wild type, the lifetimes and/or open probabilities of those shown in red were greater, and the lifetime and open probability of K82A (purple) were less.

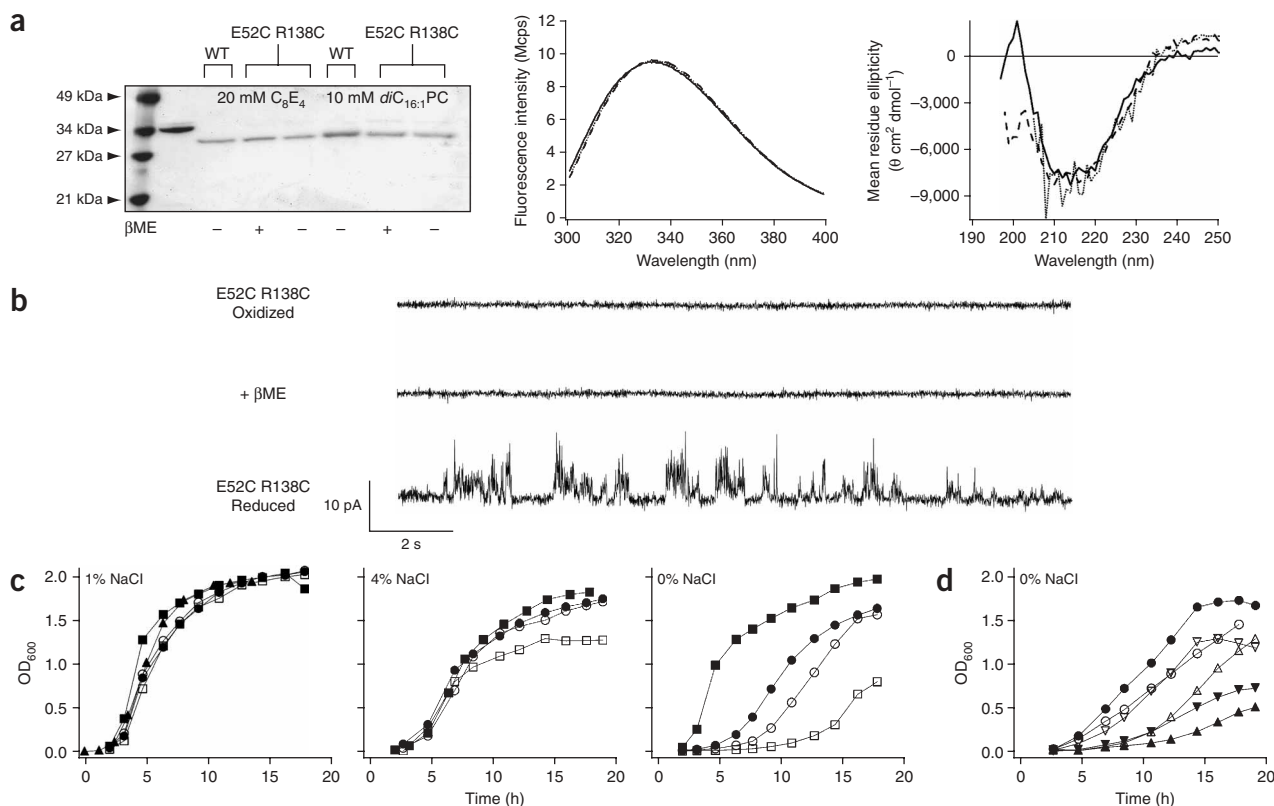


**Figure 6** Reversible blockage of channel properties by disulfide formation in place of the central salt bridge of OmpA. **(a)** Folding of wild-type (WT) and E52C R138C mutant OmpA in  $C_8E_4$  micelles and  $d/C_{16:1}PC$  bilayers. SDS-PAGE shift assay (top), tryptophan fluorescence (bottom left) and far UV CD (bottom right) of OmpA refolded in 20 mM  $C_8E_4$  or 10 mM  $d/C_{16:1}PC$  vesicles in the presence and absence of 0.2%  $\beta$ ME. **(b)** Single-channel recordings of E52C R138C mutant in planar lipid bilayers in the oxidized (upper trace) and reduced (lower trace) form in 1 M KCl at +100 mV.  $\beta$ ME alone does not induce any current fluctuations across planar lipid bilayers (middle trace). **(c)** Comparison of the growth behavior of *E. coli* BL21(DE3) (■), BL21(DE3) mutant (□,  $\Delta lamB$  *OmpF::Tn5*  $\Delta ompA$   $\Delta ompC$ ), BL21(DE3) mutant expressing the plasmid-coded OmpA wild type (●), E52C R138C mutant (▲) and transmembrane domain of OmpA (○, OmpA<sub>1-176</sub>) in LB medium with different NaCl concentrations. **(d)** Growth curves of *E. coli* BL21(DE3) cells expressing wild type (●), E52C R138C (▲), and the transmembrane domain of E52C R138C mutant (▼) OmpA in the absence (closed symbols) and presence (open symbols) of  $\beta$ ME.

that assumed a two-state (open-closed) first-order kinetic model (Fig. 5)<sup>26</sup>. The open probability ( $P_o$ ) was 10.5%.

Mutants E52Q and R138A, in which the salt bridge was disrupted, had higher channel activities than wild type (Figs. 4 and 5). The open lifetimes and open probabilities increased to  $138 \pm 4$  ms and to 48 and 17% for R138A and E52Q, respectively. However, the mean conductance values of these mutants ( $34 \pm 27$  and  $33 \pm 28$  pS, respectively) were similar to that of wild type. The open lifetime of E52Q was also similar to that of wild type. The mutants E128Q and E128A, in which the electrostatic interaction between Arg138 and Glu128 was removed, showed single-channel activities that were very similar to that of wild type. The open lifetimes and probabilities of E128Q and E128A were 100 to 110 ms and 9 to 11%, respectively, as were those of the wild type. Again, the mean conductance values were in the 30-pS range, which is not significantly different from that of wild type. By contrast, the channel activity of the K82A mutant was noticeably different from that of wild type: the open lifetime of  $57 \pm 2$  ms was shorter and the open probability of 6.7% was smaller than the corresponding values of the wild-type channel. These results indicate that Lys82 contributes to the opening of the OmpA ion channel, but Glu128 is an unlikely contributor to the channel-opening mechanism.

### Gate disulfide cross-link blocks channel function

To confirm the gating role of the salt bridge Glu52-Arg138 in the channel activity of OmpA and to investigate its functional significance *in vivo*, we prepared the double cysteine mutant E52C R138C to permanently close the gate by disulfide bond formation. The purified double cysteine mutant correctly refolded in 20 mM tetraethylene glycol monoethyl ether ( $C_8E_4$ ) detergent micelles in the presence or absence of the reducing agent  $\beta$ -mercaptoethanol ( $\beta$ ME) (Fig. 6a). Without boiling, the refolded mutant migrated as a 30 kDa form, and the tryptophan fluorescence and far UV CD spectra are identical to those of the wild type. The folded structure was maintained after reconstitution into  $d/C_{16:1}PC$  vesicles by dialysis (Fig. 6a). The addition of  $\beta$ ME modified the gel-migration patterns of boiled samples of the full-length E52C R138C mutant and its transmembrane domain (E52C R138C<sub>1-176</sub>) relative to those without the reducing agent, which indicates that the disulfide bond was formed between the two cysteine residues (Supplementary Fig. 2 online). When proteoliposomes containing the E52C R138C mutant were added to the *cis* compartment, a flat baseline with no channel activity was observed (Fig. 6b). Although the procedures of voltage shutdown, addition of 5- $\mu$ l aliquots of proteoliposomes, extensive mixing, equilibration, and reapplication of the voltage were repeated several times in 30-min

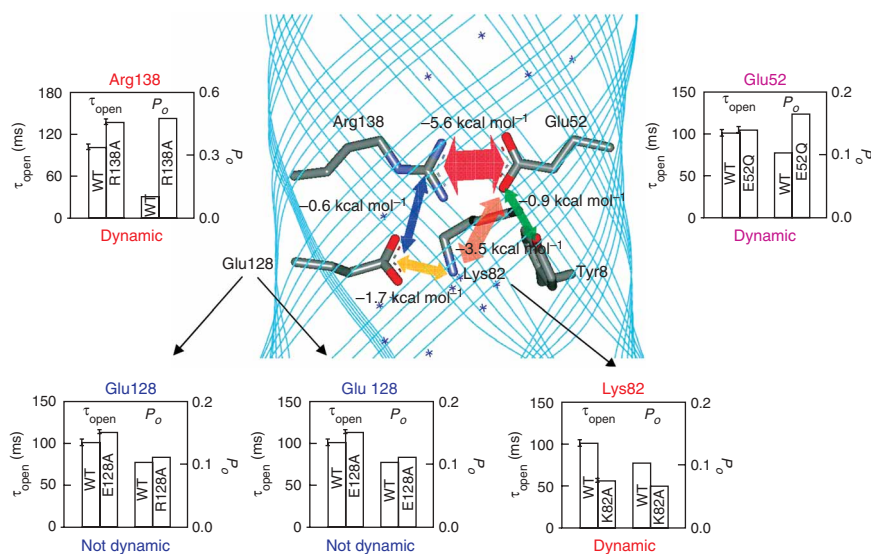


**Figure 7** Correlations between pair-wise side chain interactions, single-channel openings and conformational dynamics measured by NMR relaxation suggest a self-consistent model for the opening of the OmpA channel. Pair-wise interaction energies from double-mutant cycles (double arrows) and single-channel data of single mutants (boxes) of residues in the gate region are indicated. The residues labeled in red show conformational exchange on the microsecond to millisecond timescale. The nearest neighbor of the purple-labeled residue Glu52 shows conformational exchange (by NMR relaxation), but the blue-labeled residue Glu128 does not<sup>37</sup>. Color scheme of arrows is same as in **Figure 3**.

cycles, no single-channel events were observed for several hours of recording. On the other hand, when the protein was reduced by adding  $\beta$ ME to the buffer solution (1% in reconstitution buffer; 0.2% in both chambers), frequent channel openings were observed immediately after applying the +100-mV potential (**Fig. 6b**).  $\beta$ ME without protein did not induce any baseline fluctuations (**Fig. 6b**). The current fluctuations representing the single-channel activity of the E52C R138C mutant lasted for 2 to 5 min in several repeated experiments.

### Physiological consequences of OmpA channel gating

To test whether blocking the gate by forming a cysteine cross-link has physiological consequences *in vivo*, we followed the growth of BL21(DE3) ( $[\Delta lamB ompF::Tn5 \Delta ompA \Delta ompC]$ ) *E. coli* cells transformed with E52C R138C mutant DNA under different osmotic conditions. This strain of *E. coli*, which lacks the main porins and wild-type OmpA, grew very slowly when not transformed and when transformed with E52C R138C mutant OmpA in LB medium in the absence of added NaCl. To investigate this growth response to a hypo-osmotic environment in further detail, we grew six different *E. coli* cultures in parallel. Each culture was transformed with the plasmid encoding wild-type OmpA, the transmembrane domain of wild-type OmpA (OmpA<sub>1-176</sub>), E52C R138C mutant, the transmembrane domain of E52C R138C mutant (E52C R138C<sub>1-176</sub>), or not transformed at all. Standard *E. coli* BL21(DE3), that is cells containing the normal complement of porins, were included in these series as positive controls. When grown in LB medium containing 1% NaCl and induced with 1 mM IPTG, no growth differences of the six cultures were observed (**Fig. 6c**). Wild-type and mutant OmpAs were biosynthetically incorporated into the outer membrane under reducing and oxidizing conditions (**Supplementary Fig. 3** online). When the precultured cells were diluted 500 times in LB medium with high (4% NaCl, hyperosmotic) or low (0% NaCl, hypo-osmotic) concentra-

tions of added NaCl, the growth of the porin- and OmpA-deleted *E. coli* cells was severely impaired, especially in media with no added NaCl (**Fig. 6c**). The expression of wild-type OmpA effectively rescued the growth defect of the host cells. The expression of OmpA<sub>1-176</sub> showed a similar effect, but to a lesser extent. Expression of the major porin OmpF in the same *E. coli* strain induced a similar growth enhancement (**Supplementary Fig. 4** online). On the other hand, *E. coli* cells expressing E52C R138C or E52C R138C<sub>1-176</sub> showed growth defects that were even more severe than those of host cells, which were not transformed (**Fig. 6d**). Notably, the addition of 0.05% (v/v)  $\beta$ ME to the media enhanced the growth of cells expressing the double cysteine mutants, whereas  $\beta$ ME had an inhibitory effect on the growth of control cells that expressed wild-type OmpA. As a further control, we also made the E52C K82C mutant, which did not inhibit growth in 0% NaCl (**Supplementary Fig. 5** online). Variation of the osmotic pressure using different sucrose instead of salt concentrations yielded similar effects (**Supplementary Fig. 6** online), which implies that the observed variations in growth are mainly due to regulation of the osmotic stress rather than electrostatic effects by functional OmpA, and also that this regulation is ablated by the cross-linked double cysteine mutant of OmpA. In conclusion, functional OmpA can substitute for the physiological role of porins when cells are subjected to osmotic stress. The double cysteine mutant cannot fulfill this function under oxidizing conditions, but it works almost as well as the wild type under reducing conditions. These physiological data *in vivo* are fully consistent with OmpA working as a pore that involves the central salt bridge, and thus they completely agree with the single-channel recordings obtained *in vitro*.

### DISCUSSION

This work reveals that electrostatic interactions in the gating region have an important role in the thermodynamic stability of OmpA (**Fig. 7** and **Table 1**). The magnitude of  $-5.6 \pm 0.4$  kcal mol<sup>-1</sup> for the Glu52-Arg138 interaction makes this salt bridge one of the most strongly interacting ion pairs that has been reported so far for any protein. Interaction energies of salt bridges in water-soluble proteins determined by double-mutant cycle or pK<sub>a</sub> shift analysis range from 0 to  $-5$  kcal mol<sup>-1</sup> (refs. 3,27–30). Among these, the strongest salt-bridge interactions are those that are buried deep in hydrophobic cores of proteins. Coulombic forces are thought to dominate over desolvation costs in low-dielectric environments<sup>3,28,31</sup>. We performed an analysis of the solvent accessibility of the crystal structure of OmpA and found that the network of the four charged residues and three aromatic residues (Tyr8, Tyr94 and Phe40) that form the gate (**Fig. 1a**) is deeply buried, with only 2.6% of the total surface area exposed to solvent. The electrostatic neutrality of the charge tetrad and the highly polarizable electronic states of the surrounding aromatic residues presumably significantly reduce the desolvation cost of the residues in the central gating region of OmpA. In addition, cation- $\pi$  interactions between Arg138 and Phe40 (identified by CAPTURE<sup>32</sup>) and the stacked arrangement of carboxylate ions over the aromatic

side chains (Phe40, Tyr94 and Glu52) may further stabilize the Glu52-Arg138 interaction<sup>33</sup>.

In a marked contrast, the small interaction energies between the vicinal side chains Tyr8 and Glu128 and the main salt bridge ( $-0.5$  to  $-1.0$  kcal mol<sup>-1</sup>) are comparable to the thermal energy  $RT$ , which implies that the Tyr8-Glu52 and Glu128-Arg138 interactions are fluctuating rather than forming stable bonds. Our measurements of side chain interactions further show that Lys82 must have a unique role in the pore-opening mechanism. The ammonium group of Lys82 is beyond the salt bridge-forming range from the carboxylate groups of Glu52 and Glu128 (Fig. 1), if a cut-off distance of 4 Å is used to define a salt bridge<sup>31</sup>. Nevertheless, the interaction between Lys82 and Glu52 is quite strong, and though smaller, its value is comparable to that of the Glu52-Arg138 interaction ( $-3.5 \pm 0.3$  versus  $-5.7 \pm 0.4$  kcal mol<sup>-1</sup>, respectively). This indicates that some residues in the gate of OmpA can assume other conformations in addition to those revealed in the static crystal structure. A second point is that Lys82 is biased to interact with Glu52 rather than Glu128 ( $\Delta\Delta G_{\text{inter}} = -3.5 \pm 0.3$  kcal mol<sup>-1</sup> for Lys82-Glu52 versus  $-1.7 \pm 0.5$  kcal mol<sup>-1</sup> for Lys82-Glu128), although Glu128 is closer to Lys82 than Glu52 in the crystal structure. Apparently, Lys82 is able to form a transient salt bridge with Glu52 and thereby perturb the closed form of the Glu52-Arg138 gate. This conformational transition would require motions of considerable amplitudes from both residues. The long flexible arm of the Lys82 side chain seems to be particularly well suited to undergo a relatively large-amplitude motion without a significant perturbation of the  $\beta$ -barrel backbone.

To the best of our knowledge, double-mutant cycle analysis has not been used to study side chain interactions in any membrane protein until now. The method requires that the side chains of interest are not interacting in the unfolded state; the following arguments strongly support this notion. First, the CD spectra in Figure 2 do not show any indication of partial folding or aggregation in the denatured state. We also showed previously that OmpA is completely dissociated from the membrane in this state<sup>24</sup>. Second, an NMR study of the unfolded state of OmpX, which is an eight-stranded  $\beta$ -barrel membrane protein that is similar to OmpA, showed that the protein is completely denatured in 8 M urea, except for two short segments of consecutive residues<sup>34</sup>. Third,  $m$  values such as those reported in Table 1 can be correlated with the extent of exposed hydrophobic surface area upon unfolding<sup>35</sup>. The  $\Delta\Delta m$  values of each double-mutant cycle vanish (Supplementary Fig. 7 online), which shows that the same (full) number of residues must be exposed to solvent in the denatured states of all proteins in each cycle. A more detailed description of these results can be found in Supplementary Results online.

The mean conductance values of all mutants and wild-type OmpA reported here were  $\sim 30$  pS, albeit with relatively large error distributions. Therefore, the mutations do not affect the conductivity of the pore, but rather its gating. These conductance values are substantially smaller than the  $\sim 60$  pS previously reported for this channel<sup>14,16</sup>, most likely because the current measurements were performed at  $\sim 17$  °C, compared with  $\sim 22$  °C in the previous reports. Indeed, a recent study indicates that the conductance of the OmpA channel is strongly temperature dependent<sup>15</sup>.

The increased channel activity of the E52Q and R138A mutants relative to the wild type implies that the Glu52-Arg138 salt bridge serves as a gate of the OmpA channel, as expected from molecular dynamics simulations<sup>21</sup>. Our data show that a strong correlation exists between the activity of channel mutants and the strength of the interaction energies of the proposed open-gate ion pairs Glu128-Arg138 and Glu52-Lys82 (Fig. 7). The interaction between Arg138

and Glu128 is very weak ( $-0.6$  kcal mol<sup>-1</sup>), and likewise the mutation of Glu128 to glutamine or alanine does not change the channel activity very much. However, the interaction between Glu52 and Lys82 is quite strong ( $\Delta\Delta G_{\text{inter}} = -3.5$  kcal mol<sup>-1</sup>), and likewise the K82A mutation leads to 40–50% decreases of the open lifetime and probability. Apparently, Lys82 serves as a charge acceptor in the open state and, when removed by mutation, decreases the open-state lifetime and probability. The alternative opening mechanism, which has been proposed on the basis of modeling and molecular dynamics simulations and which involves the formation of a salt bridge between Glu128 and Arg138 (ref. 21), does not seem to be cardinal: the interaction between these residues is weak, and mutation of Glu128 to glutamine or alanine does not alter channel activity.

According to previous NMR experiments and molecular dynamics simulations, the  $\beta$ -barrel backbone of the OmpA transmembrane domain is quite rigid, showing only small amplitude fluctuations on the picosecond timescale<sup>20,21,36</sup>. More recent NMR relaxation experiments have shown that despite this rigid frame, some residues in the barrel interior undergo conformational exchange on the microsecond to millisecond timescale<sup>37</sup>. The residues that show the most pronounced conformational exchange in the gate region are Lys82 and Arg138 (Fig. 7). Glu52 does not show conformational exchange by itself, but its nearest neighbor, Met53, does. Glu128 does not show any conformational exchange, and its nearest neighbors do not either. Therefore, Glu128 likely adopts only one conformation. Combining the structural dynamics information from NMR with the current thermodynamic and single-channel results reveals the following correlations: first, the dynamic charge pairs Arg138-Glu52 and Lys82-Glu52 interact more strongly than the less dynamic pairs Glu128-Arg138 and Glu128-Lys82 (Fig. 7), and second, mutations of the conformationally active residues Arg138 and Lys82 lead to stable alternative associations with the (relatively) conformationally active Glu52 and thereby stabilize the open and closed forms of the channel gate, respectively. Therefore, all three sets of data—thermodynamics of side chain interactions, conformational dynamics, and ion-channel activity—indicate that the gate opens by Lys82 moving toward Glu52, destabilizing the obstructing gate salt bridge Arg138-Glu52 and forming the alternate open-state salt bridge Lys82-Glu52. This mechanism does not exclude (but it certainly does not require) the presence of an additional interaction between Arg138 and Glu128.

The present work confirms that the residues Glu52 and Arg138 indeed form a gate for ion passage through the barrel lumen of OmpA by showing that the single-channel activity of the double-cysteine mutant E52C R138C is blocked by the disulfide bond but observed when this bond is broken by reduction. Growth of porin-deleted cells correlates with the pore activity of OmpA. Expressed OmpA rescues the growth defect of the host cells under osmotic stress induced by high or low salt or sucrose. Cells expressing E52C R138C mutant OmpA in nonreducing medium with no added NaCl grow even slower than nontransformed cells, which shows that the disulfide block has physiological significance. Reduction of the Cys52-Cys138 disulfide relieves this block. In spite of the deleted major porins, the host strain does not show growth defects under iso-osmotic conditions. This may be due to minor cryptic porins<sup>38</sup>, which apparently cannot rescue growth defects under hypo- or hyperosmotic conditions.

Various osmoregulatory processes take place in the outer membranes of Gram-negative bacteria<sup>39,40</sup>. For example, the relative expression of OmpF and OmpC are regulated in response to different osmotic pressures by a well-characterized two-component regulation system. The sensitivity of cell growth to salt shown in our study is likely due to lack of the porin that is normally responsible for this task.

OmpA and the closely related OprF from *Pseudomonas aeruginosa* have been classified as ‘slow porins’ because they let several monosaccharides permeate about two orders of magnitude more slowly than the regular porin OmpF<sup>11</sup>. OmpA forms two conductance states in planar lipid bilayers<sup>16</sup>. The smaller conductance state (~60–80 pS) requires only the N-terminal eight-stranded  $\beta$ -barrel, but the larger conductance state (~260–320 pS), which is thought to be responsible for the slow porin activity<sup>11</sup>, also requires the C-terminal domain. Notably, the transmembrane domain alone stimulates the growth of transformed cells almost as well as the full-length protein (Fig. 6c). Cells expressing the E52C R138C<sub>1–176</sub> transmembrane domain mutant show a severe growth defect as well, but are rescued by the addition of  $\beta$ ME. These results suggest that the transmembrane domain, or equivalently the small-channel activity, is sufficient to protect the cells from osmotic stress. However, it is not clear whether ions, water or small organic solutes are the primary physiological diffusants in osmoprotection by OmpA.

The gating of OmpA by switching a tight salt bridge from a closed state to an open state is so far unique among outer-membrane protein channels. Other outer-membrane proteins such as the trimeric porins have wide water-filled lumina and are often gated by voltage<sup>41</sup>. However, a structural homology model of the transmembrane domain of OprF has recently shown that this protein has a cluster of acidic and basic residues surrounded by aromatic residues in its proposed gate region<sup>42</sup>. According to this model, a gating salt bridge exists between Glu8 and Lys121. The experimental channel activities of *P. aeruginosa* and *P. fluorescens* OprFs are consistent with the notion that OmpA and OprF are structural and functional orthologs.

In conclusion, we have presented a new method for comprehensive thermodynamic analysis of the electrostatic organization of the core of membrane proteins, which in this case was used to elucidate the gating mechanism of an ion-conducting channel. The method should prove to be quite general and could potentially be used to study side chain interactions in the catalytic mechanisms of other ion channels and nonchannel membrane proteins. When applied to helical membrane proteins, some adjustments will have to be made. Different denaturant mixtures will have to be explored to ensure complete disruption of the interacting side chains in the denatured states. However, we do not think that this is a significant limitation; substantial progress has been made recently toward establishing conditions for the reversible folding and unfolding of helical membrane proteins, including light sensors and receptors<sup>43–45</sup>. Given these folding protocols, we believe that our methods are most useful for analyzing polar interactions in membrane proteins. The analysis of nonpolar interactions may be obscured by competing interactions with the solvent in denaturant mixtures that are useful for helical membrane proteins. We expect that a wealth of new chemical biological information on membrane proteins will emerge from the use and further development of these methods. Polar interactions are important to study because they often confer specificity to folding and are the most significant contributors to many catalytic mechanisms in membrane-bound enzymes, channels and transporters<sup>5,44,46</sup>.

## METHODS

**Protein expression and purification.** Site-directed mutagenesis was carried out using the QuickChange kit (Stratagen) and the plasmid pET1113 as a template<sup>47</sup>. The vector containing the gene encoding wild-type or mutated pro-OmpA was transformed into BL21(DE3) [ $\Delta lamB$  *ompF::Tn5*  $\Delta ompA$   $\Delta ompC$ ]<sup>48</sup>. Wild-type and mutant OmpA proteins were extracted and purified in the unfolded form in 8 M urea from the outer membranes of *E. coli*, as described in **Supplementary Methods** online.

**Fitting of unfolding curves.** Urea-induced equilibrium unfolding was monitored by computing the average emission wavelength  $\langle \lambda \rangle$ . Angled brackets denote a weighted average wavelength defined as  $\langle \lambda \rangle = \sum (F_i \lambda_i) / \sum (F_i)$ .  $\lambda_i$  and  $F_i$  are the wavelength and the corresponding fluorescence intensity, respectively, at the *i*th measuring step in a spectrum. The unfolding curves, normalized to unfolded fraction, were fitted to the two-state model (**Supplementary Methods**). The free energy of unfolding is obtained using the fitted  $C_m$  and  $m$  in

$$\Delta G_{u,H_2O}^0 = mC_m \quad (3)$$

where  $C_m$  is the urea concentration at which the fractions of folded and unfolded states are equal and  $m$  is a thermodynamic parameter representing the cooperativity of unfolding.

**Single-channel measurements in planar lipid bilayers.** Planar lipid bilayers were prepared from a 15  $\mu\text{g ml}^{-1}$  solution of *di*PhPC (Avanti Polar Lipids) in *n*-decane (Aldrich). The lipid solution was painted on a 500- $\mu\text{m}$ -diameter hole in a Teflon partition separating two 1.5-ml compartments that were filled with 1 M KCl solution (10 mM Tris-HCl, pH 7.4). A chlorided silver electrode was immersed in each compartment; the front (*cis*) side was grounded and the rear (*trans*) side was connected to an Axo-Patch 200B amplifier (Axon Instruments). The formation of a planar lipid bilayer was tested by optical reflectance, resistance and capacitance. OmpA was refolded in a 20-mM  $\text{C}_8\text{E}_4$  micellar solution (10 mM glycine, pH 10.0) overnight at a final protein concentration of 40  $\mu\text{g ml}^{-1}$ . *Di*C<sub>16:1</sub>PC (10 mM) and a small amount of additional  $\text{C}_8\text{E}_4$  were mixed with the refolding product, which was then dialyzed against an excess buffer solution (10 mM glycine, pH 9.2, 0.5 mM EDTA) for 48 h. Reconstituted OmpA (5  $\mu\text{l}$ ) was added and stirred in the *cis* compartment after bilayer preparation. After a few minutes of equilibration, 100 mV of voltage was applied in the *trans* compartment, and single-channel activity was recorded on magnetic medium. For single-channel recordings of the oxidized E52C R138C mutant, the reconstituted OmpA was added to the *cis* compartment. For single-channel recordings of the reduced E52C R138C mutant, 1% of  $\beta$ ME was added to the reconstituted OmpA solution, which was then incubated for 1 h at 37 °C. After the bilayer was formed, 0.2% of  $\beta$ ME was added to both stirred compartments. The reduced E52C R138C mutant OmpA was added to the *cis* compartment and stirred again. Room temperature was  $17 \pm 1$  °C throughout these measurements.

**Single-channel analysis.** Single-channel data were filtered at 100 Hz by an eight-pole low-pass filter and digitized at 1 kHz. From a power spectrum of unfiltered data, no significant power was observed at frequencies higher than 100 Hz, which indicated that applying the low-pass filter did not affect our data analysis. The single-channel events were analyzed interactively using IGOR-PRO software (WaveMetrics) to obtain the conductance and open-time values. The results from the interactive analysis were compared to those from power spectral analysis<sup>49</sup>, and they agreed with each other within ~10–15% error limits (data not shown). The data were collected from 5 to 15 independent experiments, except for the E128A mutant data, which were analyzed from 2 independent experiments.

***E. coli* growth assay under osmotic stress.** The *E. coli* BL21(DE3) mutant strain ([ $\Delta lamB$  *ompF::Tn5*  $\Delta ompA$   $\Delta ompC$ ]) that was transformed with the plasmids encoding wild-type OmpA, E52C R138C mutant, and the transmembrane domains of wild-type OmpA (OmpA<sub>1–176</sub>) and E52C R138C (E52C R138C<sub>1–176</sub>) were initially grown in LB medium whose composition was 0.1% ampicillin (Fisher Scientific), 10% Bacto-tryptone (Becton-Dickinson and Co.), 5% yeast extract (Becton-Dickinson and Co.) and 1% NaCl (all in w/v) at 37 °C overnight in the presence of 1.0 mM IPTG (EM Science). Nontransformed *E. coli* was also grown in the absence of ampicillin as a control. The grown cultures were diluted 500 times in LB medium containing 1% Bacto-tryptone and 0.5% yeast extract, but with different NaCl or sucrose concentrations. Under each condition, the cultures were grown at 37 °C in the presence of 0.5 mM IPTG. The growth in LB medium containing 1% NaCl and 0.5 mM IPTG using the same dilution factor at the start of the incubation was also tested as a positive control. Cell growth was monitored by measuring the

optical density at 600 nm (OD<sub>600</sub>) in time intervals of 45–90 min. The expression and localization of the proteins was tested by SDS-PAGE of *E. coli* outer membranes.

**Accession codes.** Protein Data Bank: the crystal structure of the OmpA transmembrane domain is under the accession code 1QJP.

*Note: Supplementary information is available on the Nature Chemical Biology website.*

#### ACKNOWLEDGMENTS

We thank D. Reinhart for technical assistance, M. Kim and D. Cafiso (University of Virginia) for sharing the BL21(DE3) ( $[\Delta lamB ompF::Tn5 \Delta ompA \Delta ompC]$ ) strain, and the late R. Kadner (University of Virginia) and R. Kaback (University of California Los Angeles) for helpful suggestions. This work was supported by US National Institutes of Health grant GM51329.

#### AUTHOR CONTRIBUTIONS

H.H. performed all experiments, H.H. and L.K.T. designed the experiments and wrote the manuscript, and G.S. participated in the electrophysiological experiments.

#### COMPETING INTERESTS STATEMENT

The authors declare that they have no competing financial interests.

Published online at <http://www.nature.com/naturechemicalbiology>  
Reprints and permissions information is available online at <http://npg.nature.com/reprintsandpermissions/>

- Perutz, M.F. Electrostatic effects in proteins. *Science* **201**, 1187–1191 (1978).
- Lee, L.P. & Tidor, B. Barstar is electrostatically optimized for tight binding to barnase. *Nat. Struct. Biol.* **8**, 73–76 (2001).
- Waldburger, C.D., Schildbach, J.F. & Sauer, R.T. Are buried salt bridges important for protein stability and conformational specificity? *Nat. Struct. Biol.* **2**, 122–128 (1995).
- Yang, A.-S. & Honig, B. Electrostatic effects on protein stability. *Curr. Opin. Struct. Biol.* **2**, 40–45 (1992).
- Engelman, D.M. *et al.* Membrane protein folding: beyond the two stage model. *FEBS Lett.* **555**, 122–125 (2003).
- Call, M.E., Pyrdol, J., Wiedmann, M. & Wucherpennig, K.W. The organizing principle in the formation of the T cell receptor-CD3 complex. *Cell* **111**, 967–979 (2002).
- Kim, J.M. *et al.* Structural origins of constitutive activation in rhodopsin: role of the K296/E113 salt bridge. *Proc. Natl. Acad. Sci. USA* **101**, 12508–12513 (2004).
- Jiang, Y., Ruta, V., Chen, J., Lee, A. & MacKinnon, R. The principle of gating charge movement in a voltage-dependent K<sup>+</sup> channel. *Nature* **423**, 42–48 (2003).
- Lecar, H., Larsson, H.P. & Grabe, M. Electrostatic model of S4 motion in voltage-gated ion channels. *Biophys. J.* **85**, 2854–2864 (2003).
- Koebnik, R., Locher, K.P. & Van Gelder, P. Structure and function of bacterial outer membrane proteins: barrels in a nutshell. *Mol. Microbiol.* **37**, 239–253 (2000).
- Nikaido, H. Molecular basis of bacterial outer membrane permeability revisited. *Microbiol. Mol. Biol. Rev.* **67**, 593–656 (2003).
- Vogel, H. & Jähnig, F. Models for the structure of outer-membrane proteins of *Escherichia coli* derived from Raman spectroscopy and prediction methods. *J. Mol. Biol.* **190**, 191–199 (1986).
- Sugawara, E. & Nikaido, H. Pore-forming activity of OmpA protein of *Escherichia coli*. *J. Biol. Chem.* **267**, 2507–2511 (1992).
- Saint, N., De, E., Julien, S., Orange, N. & Molle, G. Ionophore properties of OmpA of *Escherichia coli*. *Biochim. Biophys. Acta* **1145**, 119–123 (1993).
- Zakharian, E. & Reusch, R.N. Outer membrane protein A of *Escherichia coli* forms temperature-sensitive channels in planar lipid bilayers. *FEBS Lett.* **555**, 229–235 (2003).
- Arora, A., Rinehart, D., Szabo, G. & Tamm, L.K. Refolded outer membrane protein A of *Escherichia coli* forms ion channels with two conductance states in planar lipid bilayers. *J. Biol. Chem.* **275**, 1594–1600 (2000).
- Schweizer, M., Hindennach, I., Garten, W. & Henning, U. Major proteins of the *Escherichia coli* outer cell envelope membrane. Interaction of protein II with lipopolysaccharide. *Eur. J. Biochem.* **82**, 211–217 (1978).
- Prasadarao, N.V. *et al.* Outer membrane protein A of *Escherichia coli* contributes to invasion of brain microvascular endothelial cells. *Infect. Immun.* **64**, 146–153 (1996).
- Pautsch, A. & Schulz, G.E. Structure of the outer membrane protein A transmembrane domain. *Nat. Struct. Biol.* **5**, 1013–1017 (1998).
- Arora, A., Abildgaard, F., Bushweller, J.H. & Tamm, L.K. Structure of outer membrane protein A transmembrane domain by NMR spectroscopy. *Nat. Struct. Biol.* **8**, 334–338 (2001).
- Bond, P.J., Faraldo-Gomez, J.D. & Sansom, M.S. OmpA: a pore or not a pore? Simulation and modeling studies. *Biophys. J.* **83**, 763–775 (2002).
- Fersht, A.R., Matouschek, A. & Serrano, L. The folding of an enzyme. I. Theory of protein engineering analysis of stability and pathway of protein folding. *J. Mol. Biol.* **224**, 771–782 (1992).
- Pautsch, A. & Schulz, G.E. High-resolution structure of the OmpA membrane domain. *J. Mol. Biol.* **298**, 273–282 (2000).
- Hong, H. & Tamm, L.K. Elastic coupling of integral membrane protein stability to lipid bilayer forces. *Proc. Natl. Acad. Sci. USA* **101**, 4065–4070 (2004).
- Kleinschmidt, J.H. & Tamm, L.K. Folding intermediates of a  $\beta$ -barrel membrane protein. Kinetic evidence for a multi-step membrane insertion mechanism. *Biochemistry* **35**, 12993–13000 (1996).
- Colquhoun, D. & Hawkes, A.G. in *Single Channel Recording* (eds. Sakmann, B. & Neher, E.) 397–482 (Plenum, New York, 1995).
- Horowitz, A., Serrano, L., Avron, B., Bycroft, M. & Fersht, A.R. Strength and cooperativity of contributions of surface salt bridges to protein stability. *J. Mol. Biol.* **216**, 1031–1044 (1990).
- Tissot, A.C., Vuilleumier, S. & Fersht, A.R. Importance of two buried salt bridges in the stability and folding pathway of barnase. *Biochemistry* **35**, 6786–6794 (1996).
- Marqusee, S. & Sauer, R.T. Contributions of a hydrogen bond/salt bridge network to the stability of secondary and tertiary structure in  $\lambda$  repressor. *Protein Sci.* **3**, 2217–2225 (1994).
- Anderson, D.E., Bechtel, W.J. & Dahlquist, F.W. pH-induced denaturation of proteins: a single salt bridge contributes 3–5 kcal/mol to the free energy of folding of T4 lysozyme. *Biochemistry* **29**, 2403–2408 (1990).
- Kumar, S. & Nussinov, R. Fluctuations in ion pairs and their stabilities in proteins. *Proteins* **43**, 433–454 (2001).
- Gallivan, J.P. & Dougherty, D.A. Cation- $\pi$  interactions in structural biology. *Proc. Natl. Acad. Sci. USA* **96**, 9459–9464 (1999).
- Thompson, S.E. & Smithrud, D.B. Carboxylates stacked over aromatic rings promote salt bridge formation in water. *J. Am. Chem. Soc.* **124**, 442–449 (2002).
- Tafer, H., Hiller, S., Hilty, C., Fernandez, C. & Wuthrich, K. Nonrandom structure in the urea-unfolded *Escherichia coli* outer membrane protein X (OmpX). *Biochemistry* **43**, 860–869 (2004).
- Myers, J.K., Pace, C.N. & Scholtz, J.M. Denaturant m values and heat capacity changes: relation to changes in accessible surface areas of protein unfolding. *Protein Sci.* **4**, 2138–2148 (1995).
- Bond, P.J. & Sansom, M.S. Membrane protein dynamics versus environment: simulations of OmpA in a micelle and in a bilayer. *J. Mol. Biol.* **329**, 1035–1053 (2003).
- Tamm, L.K., Abildgaard, F., Arora, A., Blad, H. & Bushweller, J.H. Structure, dynamics and function of the outer membrane protein A (OmpA) and influenza hemagglutinin fusion domain in detergent micelles by solution NMR. *FEBS Lett.* **555**, 139–143 (2003).
- Prilipov, A., Phale, P.S., Koebnik, R., Widmer, C. & Rosenbusch, J.P. Identification and characterization of two quiescent porin genes, *nmpC* and *ompN*, in *Escherichia coli* B<sup>F</sup>. *J. Bacteriol.* **180**, 3388–3392 (1998).
- Csonka, L.N. & Hanson, A.D. Prokaryotic osmoregulation: genetics and physiology. *Annu. Rev. Microbiol.* **45**, 569–606 (1991).
- Wood, J.M. Osmosensing by bacteria: signals and membrane-based sensors. *Microbiol. Mol. Biol. Rev.* **63**, 230–262 (1999).
- Schindler, H. & Rosenbusch, J.P. Matrix protein from *Escherichia coli* outer membranes forms voltage-controlled channels in lipid bilayers. *Proc. Natl. Acad. Sci. USA* **75**, 3751–3755 (1978).
- Khalid, S., Bond, P.J., Deol, S.S. & Sansom, M.S. Modeling and simulations of a bacterial outer membrane protein: OprF from *Pseudomonas aeruginosa*. *Proteins* **63**, 6–15 (2006).
- Booth, P.J. Sane in the membrane: designing systems to modulate membrane proteins. *Curr. Opin. Struct. Biol.* **15**, 435–440 (2005).
- Bowie, J.U. Solving the membrane protein folding problem. *Nature* **438**, 581–589 (2005).
- Lau, F.W. & Bowie, J.U. A method for assessing the stability of a membrane protein. *Biochemistry* **36**, 5884–5892 (1997).
- Senes, A., Engel, D.E. & DeGrado, W.F. Folding of helical membrane proteins: the role of polar, GxxxG-like and proline motifs. *Curr. Opin. Struct. Biol.* **14**, 465–479 (2004).
- Kleinschmidt, J.H., den Blaauwen, T., Driessen, A.J. & Tamm, L.K. Outer membrane protein A of *Escherichia coli* inserts and folds into lipid bilayers by a concerted mechanism. *Biochemistry* **38**, 5006–5016 (1999).
- Prilipov, A., Phale, P.S., Van Gelder, P., Rosenbusch, J.P. & Koebnik, R. Coupling site-directed mutagenesis with high-level expression: large scale production of mutant porins from *E. coli*. *FEMS Microbiol. Lett.* **163**, 65–72 (1998).
- Neher, E. & Stevens, C.F. Conductance fluctuations and ionic pores in membranes. *Annu. Rev. Biophys. Bioeng.* **6**, 345–381 (1977).